Lab-made flexible third-generation fructose biosensors based on 0D-nanostructured transducers

Silveri, Filippo; Paolini, Davide; Della Pelle, Flavio; Bollella, Paolo; Scroccarello, Annalisa; Suzuki, Yohei; Fukawa, Eole; Sowa, Keisei; Di Franco, Cinzia; Torsi, Luisa; Compagnone, Dario

Please cite the original version:
Silveri, F., Paolini, D., Della Pelle, F., Bollella, P., Scroccarello, A., Suzuki, Y., Fukawa, E., Sowa, K., Di Franco, C., Torsi, L., & Compagnone, D. (2023). Lab-made flexible third-generation fructose biosensors based on 0D-nanostructured transducers. *Biosensors and Bioelectronics*, *237*, Article 115450. https://doi.org/10.1016/j.bios.2023.115450

Lab-made flexible third-generation fructose biosensors based on 0D-nanostructured transducers

Filippo Silveri [a,1], Davide Paolini [a,1], Flavio Della Pelle [a,*], Paolo Bollella [b,c], Annalisa Scroccarello [a], Yohei Suzuki [d], Eole Fukawa [d], Keisei Sowa [d], Cinzia Di Franco [e], Luisa Torsi [b,c,f], Dario Compagnone [a,**]

[a] *Department of Bioscience and Technology for Food, Agriculture and Environment, University of Teramo, Campus "Aurelio Saliceti" Via R. Balzarini 1, 64100 Teramo, Italy*
[b] *Department of Chemistry, University of Bari Aldo Moro, Via E. Orabona 4, 70125 Bari, Italy*
[c] *Centre for Colloid and Surface Science – University of Bari Aldo Moro, Via Edoardo Orabona 4, 70125 Bari, Italy*
[d] *Division of Applied Life Sciences, Graduate School of Agriculture, Kyoto University, Kitashirakawa Oiwake-cho, Sakyo-ku, Kyoto, 606-8502, Japan*
[e] *Istituto di Fotonica e Nanotecnologie CNR, C/o Dipartimento Interateneo di Fisica, University of Bari Aldo Moro, Via Edoardo Orabona 4, 70125 Bari, Italy*
[f] *Faculty of Science and Engineering, Åbo Akademi University, 20500 Turku Finland*

ARTICLE INFO

ABSTRACT

Herein, we report a scalable benchtop electrode fabrication method to produce highly sensitive and flexible third-generation fructose dehydrogenase amperometric biosensors based on water-dispersed 0D-nanomaterials.

The electrochemical platform was fabricated via Stencil-Printing (StPE) and insulated via xurography. Carbon black (CB) and mesoporous carbon (MS) were employed as 0D-nanomaterials promoting an efficient direct electron transfer (DET) between fructose dehydrogenase (FDH) and the transducer. Both nanomaterials were prepared in water-phase via a sonochemical approach. The nano-StPE exhibited enhanced electrocatalytic currents compared to conventional commercial electrodes.

The enzymatic sensors were exploited for the determination of D-fructose in model solutions and various food and biological samples. StPE-CB and StPE-MS integrated biosensors showed appreciable sensitivity ($\sim$150 µA cm^{-2} mM^{-1}) with µmolar limit of detection (0.35 and 0.16 µM, respectively) and extended linear range (2–500 and 1–250 µM, respectively); the selectivity of the biosensors, ensured by the low working overpotential ($+0.15$ V), has been also demonstrated. Good accuracy (recoveries between 95 and 116%) and reproducibility (RSD $\leq$8.6%) were achieved for food and urine samples.

The proposed approach because of manufacturing versatility and the electro-catalytic features of the water-nanostructured 0D-NMs opens new paths for affordable and customizable FDH-based bioelectronics.

1. Introduction

Recently, the demand for smart analytical biosensors for Point-of-Care (PoC) or Point-of-Need (PoN) dramatically increased (Byakodi et al., 2022; Cinti, 2019; Nesakumar et al., 2019; Umapathi et al., 2022). Notably, electrochemical devices offer the possibility to produce miniaturized and portable analytical tools, suitable for on-site analysis/diagnostics (Campuzano et al., 2021; Nesakumar et al., 2019; Silva-Neto et al., 2023). In this context, the bioanalytical community is moving towards device manufacturing with affordable benchtop or even office instrumentation able to ensure the needed performance.

Flexible plastics and cellulosic substrates already demonstrated their pros for electroanalytical devices development because of their great versatility, offering opportunities beyond classical screen printing (Hernández-Rodríguez et al., 2020; Rama and Abedul, 2021; Rojas et al., 2020). Among emerging user-friendly technologies, lab-made integrated electrochemical (bio)sensors, xurography, wax printing, laser-molding, thermal assembling, and inkjet printing stand out (Arduini et al.,

---

2019; Rama and Abedul, 2021). Stencil printing is an affordable and effective approach for the development of lab-made flexible (bio)electronics (Hernández-Rodríguez et al., 2020; Kongkaew et al., 2022; Tricase et al., 2023), resulting particularly suited for wearable (bio)sensors and biofuel cell fabrication. Indeed, this approach allows to produce electrodes/circuits on a large scale with specific design and shape, onto various substrates (Kay and Desmulliez, 2012; Kongkaew et al., 2022; Zavanelli et al., 2021). The potentialities of this strategy have not been completely explored yet, particularly in conjunction with other cost-effective manufacturing technologies for biosensor developments.

Most of the existing studies regarding lab-made production of PoC/PoN sensing devices focus their attention on first and second-generation enzymatic amperometric biosensors (Li et al., 2020; Mathew et al., 2020; Xia et al., 2020; Yoon et al., 2020; Zhang et al., 2021); the enzymatic direct electron transfer (DET) phenomenon has been exploited mainly for the fabrication of flexible biofuel cells (Jeerapan et al., 2020; Kong et al., 2020; Loew et al., 2022). Only few reports are claiming the development of third-generation lab-made biosensors (Hiraka et al., 2021; Jayakumar et al., 2022). Despite the widespread of glucose oxidase (GOx) within the enzymatic biosensing community, there is clear evidence that native GOx cannot perform DET at the electrode surface (Bartlett and Al-Lolage, 2018; Bollella and Katz, 2020; Schachinger et al., 2021; Wilson, 2016).

DET phenomena have been extensively investigated for several enzymes, aimed at revealing fundamental features of redox proteins for the development of third-generation biosensors (Adachi et al., 2020; Bollella, 2022; Schachinger et al., 2021). Particularly, fructose dehydrogenase (FDH) from *Gluconobacter japonicus* has been widely exploited for fructose detection (Bollella, 2022). The entire structure of FDH (PDB: 7W2J) has been revealed by using cryo-electron microscopy and single-particle analysis (Suzuki et al., 2022). FDH is a membrane-bound protein encompassing three subunits: the catalytic domain catalyzing fructose oxidation (subunit I, DH_{FDH}, containing flavin adenine dinucleotide (FAD) accepting electrons from fructose and 3Fe4S cluster), the built-in electron acceptor unit containing three heme moieties (subunit II CYT_{FDH}, in which only heme 1 and heme 2 participate to the electron transfer pathway) and subunit III, which is needed for conformational stability and is not involved in the electron transfer (Bolella et al., 2018a; Bollella et al., 2018b, 2019).

The employment of nanomaterials (NMs) represents a successful strategy to improve the features of lab-made (bio)sensors (Arduini et al., 2019). To eliminate the use of organic solvents and obtain water-soluble nano-colloids, sustainable NMs production/nanodispersions strategies are gaining interest (Naghdi et al., 2020). Recently, our group has demonstrated how different NMs can be 'produced' in water sonochemically, taking advantage of naturally/biologically occurring compounds as stabilizers; the water-dispersed NMs are easy to handle and particularly prone to nano-structuration of electrodic surfaces for sensing applications (Elfadil et al., 2023; Silveri et al., 2022). In particular, these NMs resulted effective for the modification/fabrication of stencil-printed electrodes (Bukhari et al., 2021; Elfadil et al., 2023; Rojas et al., 2022); in fact, organic solvents, normally present in NMs suspensions, can cause the dissolution and the spoilage of the conductive inks.

Several FDH-based sensors have used the enzyme in combination with NMs produced and nanostructured with conventional strategies, among these, carbon nanotubes (Bolella et al., 2018b; Bollella et al., 2021), gold nanoparticles (Bollella et al., 2019), graphene (Antiochia and Gorton, 2014; Šakinyte et al., 2015) and nano/micro-structured gold (Bollella et al., 2018a; Siepenkoetter et al., 2017; Suzuki et al., 2020). In these reports, often, chemical modification of the sensing surface with spacers and cross-linkers is needed to drive the orientation of the enzyme and minimize the distance between the cofactor and the electrode surface (Chekin et al., 2015; Gooding et al., 2011). To the best of our knowledge, the integration of FDH in flexible lab-made nano-structured sensors is not reported yet; exploring this topic in our opinion

deserve to be studied to meet the requirements for the development of affordable and accessible to end-users PoC/PoN devices (Bollella, 2022).

In this work, lab-made sensors have been manufactured through a benchtop approach, nano-structured with 0D carbon NMs produced in water, and used as transducers to give rise to FDH-based third-generation biosensors. The StPE fabrication strategy has been rationally designed to host the FDH and enhance its DET. The nano-StPEs' features and performance were carefully evaluated and compared to conventional commercial electrodes, demonstrating their exploitability as transducers for DET-based biosensing, with no need for spacers and/or cross-linkers. The 0D NMs (CB and MS) used induce an outstanding improvement of the electro-catalytic features of the biosensors, with consequent enhancement of the DET-induced catalytic current; remarkable analytical performance in terms of sensitivity, reproducibility, and repeatability has been also obtained. The nano-StPEs' were successfully challenged for the determination of D-fructose in model solutions, food and biological samples.

2. Experimental

2.1. Chemicals and samples

Sodium cholate hydrate, sodium acetate, potassium chloride, potassium ferrocyanide, potassium ferricyanide and D-fructose were purchased from Sigma Aldrich (St Louis MO, USA). Recombinat FDH (native type EC 1.1.99.11 from Gluconobacter japonicus NCBR 3260 (40 U mg^{-1}) was epressed and purified as described in previous works (Ameyama et al., 1981; Kawai et al., 2013). The FDH sample was stored in a McIlvaine buffer solution (pH 4.5, 0.1% Triton® X-100, and 1 mM 2-mercaptoethanol). Sodium phosphate monobasic monohydrate, ascorbic acid, citric acid, uric acid, glucose, sucrose, galactose, maltose, mannitol, urea, L-tyrosine, L-lysine, L-cysteine, glutathione, KCl, KNO$_3$, NaNO$_2$, NaCl, CaCl$_2$, NaHCO$_3$, MgCl$_2$, K$_2$HPO$_4$ were purchased from Sigma Aldric (St Louis, MO, USA).

Carbon graphite ink, Ag/AgCl ink, and mesoporous carbon (MS) were purchased from Sigma Aldrich (St Louis, MO, USA), while carbon black N220 (CB) was obtained from Cabot Corporation (Ravenna, Italy).

Food samples (beverages and honey) were purchased from local food markets, whereas human urine was gently donated by healthy volunteers.

Before the analysis, the samples were centrifuged at 5k g for 10 min to eliminate the impurities and then diluted in 50 mM acetate buffer solution at pH = 4.5 containing 0.1 M KCl (ABS) to fit the linear range of the relative calibration curve. Milli-Q grade water 18.2 MΩ cm^{-1} (Millipore, Bedford, MA, USA) was used to perform the experiments.

Healthy volunteers were participating in all measurements and procedures herein described without any minimal health risks, and written informed consent was received. The treatment of personal data was done in accordance with the provisions of the GDPR law 675/1996, based on Directive 95/46/EC, which aims to prevent the violation of personal integrity in the processing of personal data. There is no possibility of harm arising as a result of the conduct of the research project or when the information being collected is available from the public domain.

2.2. Apparatus

The probe sonifier SFX550 (Sonifier® SFX series; Branson Sonic Power Co., Banbury, Connecticut, USA) equipped with a 1/8" tapered Microtip (wattage Output: 550 W; frequency Output: 20 kHz) was employed for the preparation of the water-based 0D nanosuspensions.

Electrochemical experiments were carried out using a portable Potentiostat/Galvanostat/Impedance Analyzer Palmsens 4 (Palm Instruments BV, Houten, Netherlands) governed by PS trace 5.9 software.

A Silhouette Cameo cruft cutter 4 managed by the Silhouette 4.4 software (Silhouette America®, Lindon, USA) and a Thermal roll
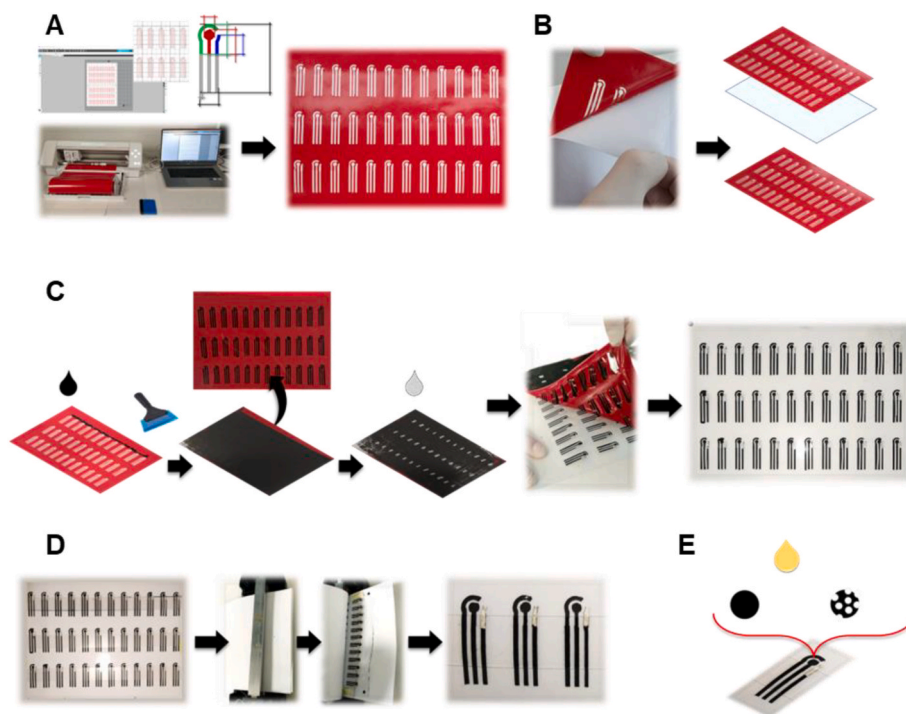
Scheme 1. Sketch of the nano-StEPs biosensors manufacturing. (**A**) Stencil-printing mask design and production via cutting plotter engraving. (**B**) Stencil-mask peeling-off and alignment onto PVC substrate. (**C**) Stencil printing of electrode contacts with carbon ink and reference electrodes finalization with silver ink. (**D**) Electrodes contact insulation by thermal lamination. (**E**) Biosensor assembling via 0D-NMs and FDH modification.

machine (Pavo 8038718 from Unbekannt) were employed for building up the Stencil-PrintEd sensors (StPE); specifications on the fabrication and dimensions of StPEs are given in section 2.3.2. Commercial screen-printed electrodes (cSPE) DRP 110 from Metrohm Dropsens (Oviedo, Spain) (Ø = 4 mm) and BASI glassy carbon electrode (GCE) (Ø = 3 mm) were employed as control transducers.

Field scanning electron microscopy (SEM) was performed with a GeminiSEM 500 (Zeiss Co., Oberkrochen, Germany). SEM micrographs were acquired using an In-Lens detector for secondary electrons; the analyses were performed on uncoated StPE-CB and StPE-MS working electrode surfaces using an acceleration potential of 3 kV and working at a distance of about 3 mm.

2.3. Biosensors manufacturing

2.3.1. Aqueous-phase 0D-nanomaterials sonochemical preparation

The CB and MS were prepared by roughly dispersing 5 mg of bulk powder material in 5 mL of a 1 mg mL^{-1} sodium cholate (SC) aqueous solution. The dispersions were then sonicated with a high-power probe sonifier (section 2.2) using a pulsed program (2 s ON, 1 s OFF) for 1 h, keeping the sample in an ice bath to avoid temperature increases over 10 °C. The obtained colloidal suspensions were then purified, centrifuging for 15 min at 20 k g to eliminate the supernatant containing the excess of SC; thus, the supernatant was discarded and the pellet was resuspended in 5 mL of water. Once resuspended the dispersion needs to be used within 1 day, while the nanomaterial can be stored as pellet (to be resuspended) for 2 weeks at +4 °C.

2.3.2. Biosensors assembling via stencil-printing/xurography

The biosensor fabrication procedure, with the pictures of the main steps and components, is reported in Scheme 1.

The in-series production of the transducers was carried out using different substrates. Smooth polyvinyl chloride (PVC) (0.18 mm; Fellowes, Itasca, Illinois, USA) was used as sensor base. Self-adhesive vinyl stencil mask (TINYYO, Parson drove, Wisbech, UK) for ink-printing was

defined with the cutting-plotter (speed balde: 10; blade power: 10, blade depth: 3) according to a multi-electrodes pattern designed with Silhouette 4.4 software. Polyethylene terephthalate-ethylene vinyl acetate laminating sheets (PET-EVA) (0.100 mm; Fellowes, Itasca, Illinois, USA) were used as insulating.

In brief, the patterned stencil mask (**A**) was stuck onto PVC sheet (**B**), and the carbon conductive ink was spread using a squeegee (**C**), allowing the formation of the working, counter, and reference electrodes according to the shape of the mask; after that, an ink curing at 60 °C for 30 min was performed. To complete the electrochemical cell, Ag/AgCl ink was gently brushed onto the respective contact to integrate the reference electrode; afterward, the stencil mask was removed, and the sheet containing the sensors underwent further curing (60 °C, 10 min). The electrodes were insulated from the contacts via thermal lamination (**D**), by laying a thermoadhesive PET-EVA sheet onto the PVC support. The working electrode surface was then modified by drop-casting 9 μL of 1 mg mL^{-1} water-based 0D-nanodispersion (section 2.3.1) (**E**); this was achieved in three steps, using a warm bulb lamp. After the NM drop-casting the nano-StPE can be stored for 2 months at 4 °C. Eventually, 4 μL of the 40 U mg^{-1} FDH suspension was deposited on the nano-StPE and left to 'interact' for 45 min in dark. The FDH suspension has been drop-casted freshly after thawing, using the biosensors within 24 h to ensure the maximum enzymatic activity.

2.4. Electrochemical measurements

The features of commercial transducers and lab-made StPEs were compared using an external counter (CE) and reference (RE) electrode; Pt wire and Ag/AgCl (3 M KCl) were used as CE and RE, respectively. Cyclic voltammetry (CV) at 5 mV s^{-1} in ABS was used to investigate the direct electron transfer (DET) process occurring at the different FDH-based biosensors; measurements have been performed in absence and presence of 10 mM D-fructose. Electrochemical impedance spectroscopy (EIS) was employed to investigate the charge transfer resistance of the sensors, using 5 mM [Fe(CN)$_6$]$^{3-/4-}$ in 0.1 M KCl as probe; the potential
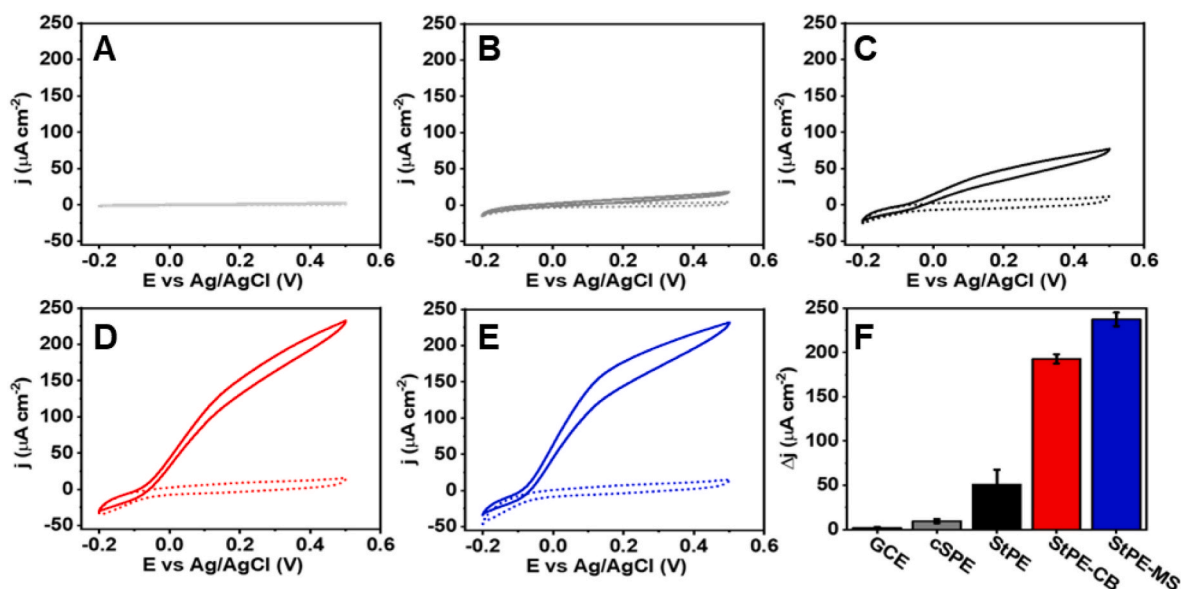
Fig. 1. Cyclic voltammograms at the FDH-based sensors obtained in ABS (dashed curves) and after the addition of 10 mM D-fructose performed with (**A**) GCE, (**B**) cSPE, (**C**) StPE, (**D**) StPE-CB, and (**E**) StPE-MS. (**F**) Current densities recorded at +0.4 V obtained with the whole set of sensors; Δj was obtained subtracting the capacitive current of the blank (ABS only) at the faradaic catalytic current obtained in presence of 10 mM fructose. Scan rate was 5 mV s^{-1}.

was fixed at the open circuit and a sinusoidal wave of 5 mV of amplitude was used, the frequency was scanned between 10^5 to 10^{-1} Hz. The Randless-equivalent circuit was employed to fit the data in the obtained Nyquist plot. Amperometry was used as biosensing technique, working at the potential of +0.15 V (vs Pseudo Ag/AgCl); in this case, the integrated sensors were used, where graphite ink acted as CE and Ag/AgCl ink as pseudo-RE (see section 2.3.2).

3. Results and discussion

This work aims to provide a viable method to build up portable FDH-based third-generation biosensors for the detection of D-fructose in food and clinical samples using benchtop technologies. To this aim, integrated transducers were fabricated through stencil-printing and xurography. Then, water-produced 0D-carbonaceous NMs were used to enhance FDH-DET catalysis. The proposed approach allows produces affordable integrated bioelectrochemical systems with customizable designs.

3.1. FDH-based StPEs catalytic performance

Initially, the electro-catalytic performance of the lab-made bare-StPE and nano-StPEs was compared with conventional transducers, namely glassy carbon (GCE) and commercial screen-printed (cSPE) electrodes. The ability to give DET reaction with FDH was investigated by using cyclic voltammetry (CV). Fig. 1A–E report CVs performed in non-turnover (dashed curves) and turnover conditions (solid curves), carried out at (**A**) GCE, (**B**) cSPE, (**C**) StPE, (**D**) StPE-CB, and (**E**) StPE-MS.

To evaluate the electrocatalytic activity from the DET reaction, the potential of onset (E_{onset}) and the density current increase (Δj) have been extrapolated from the CVs reported in Fig. 1; the Δj has been calculated considering the density current observed at + 0.4 V, to take into consideration the whole electro-catalytic wave, in agreement with the literature (Bollella et al., 2021). GCE (E_{onset} = −0.065 V; Δj = 1.9 ± 0.8 µA cm^{-2}) and cSPE (E_{onset} = −0.068 V; Δj = 9.4 ± 2.3 µA cm^{-2}) exhibited poor electrocatalytic behavior in the presence of D-fructose. Notably, the bare-StPE showed a significantly greater electrocatalytic wave, that starts at −0.090 V and rise up to a current density of 50.8 ± 16.7 µA cm^{-2} at +0.4 V. The obtained result indicates that the StPE represents a suitable platform for FDH-DET reaction, probably for the

higher roughness and surface area of the film formed with the carbon ink (see section 3.2), which allows higher enzyme loading/communication (Bolella et al., 2018b). On the other hand, from the voltammetric curves obtained for StPE-CB (**D**) and StPE-MS (**E**), it is clear how the nano-structuration of the sensing surface brought an outstanding enhancement of enzyme/electrode DET. Significantly larger electrocatalytic waves, in turnover condition, have been obtained; the latter start at −0.113 V (StPE-CB) and −0.107 V (StPE-MS) and rise to a current density of 192.7 ± 5.2 and 237.4 ± 7.7 µA cm^{-2} at +0.4 V, respectively. In addition, the electrocatalytic waves obtained at the nano-StPEs in turnover conditions have a shoulder at ∼ +0.1 V, which can be attributed to the electron release from the heme *c* moieties of the subunit II; this is in agreement with other DET reactions reported for FDH-based bioelectronics (Bolella et al., 2018b; Bollella et al., 2018a, 2021). A better comparison of the obtained catalytic current densities is reported in Fig. 1F. Notably, nano-StPEs electrocatalysis resulted also reproducible (RSD = 2.7% and 3.3% for CB and MS, respectively; n = 3). The impressive increase of the catalytic current density, along with the shift towards negative values of the onset potential, suggests that the nanostructuration of the StPE plays a key role to improve electronic communication with the enzyme. This can be attributed to the higher surface/volume ratio and the resulting more wrinkled sensing surface, offering more sites for enzyme loading and electron exchanges. Moreover, the nanostructures may play a role in driving the FDH orientation; in fact, the sensors do not need spacers or cross-linkers. The 0D-NMs ability to (i) lead to multiple interactions with FDH, (ii) shortening the distance between the enzymatic redox site has been already reported (Olloqui-Sariego et al., 2021; Sugimoto et al., 2016). A further favorable effect, reported in section 2.2, is the significant reduction in the charge-transfer resistance, which probably favors electron transfer between the FDH and the sensing surface.

The influence of the amount of the 0D-NMs on the catalytic response was investigated functionalizing the StPEs with NM amounts from 1 µg to 15 µg; Fig. S1 revealed as 9 µg of NM allow to reach the maximum catalytic current density for both StPEs-CB and StPEs-MS. Despite, the two NMs returning the maximum response at the same material amount, the NM-amount/response trend is different, probably for the different NM structural features. Indeed, CB particles are characterized by a filled structure, while MS has a porous structure; thus for CB, after reaching the optimal material amount, the carbon nanoparticles tend to
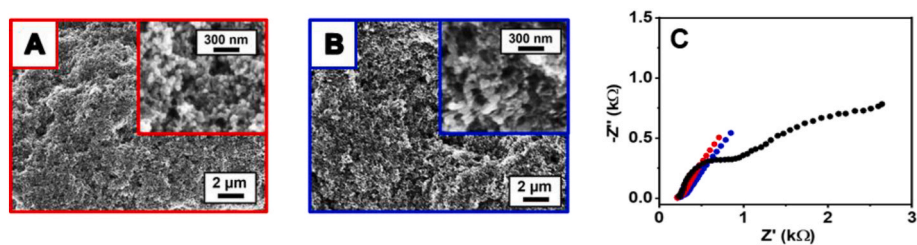
Fig. 2. SEM micrograph of the sensing surface of the (**A**) StPE-CB and (**B**) StPE-MS, signal acquisition In-lens magnification 10kx; insets report magnifications acquired at 75 k x. (**C**) Nyquist plot obtained via EIS in presence of 5 mM [Fe(CN)$_6$]$^{3-/4-}$ containing 0.1 M KCl, performed at the bare-StPE (black spots), StPE-CB (red spots), and StPE-MS (blue spots).

aggregate/compact, reducing the surface area and the sites for enzyme loading, with consequent decrease of the performance (Khodabakhshi et al., 2020; Silveri et al., 2022). On the other hand, the MS nanospheres allow to host enzyme molecules even at higher quantities of material, without losing catalytic performance, thanks to the porous structure (Park et al., 2017, 2018); however, once the optimal NM quantity is exceeded, there is a worsening of reproducibility. Therefore, as a compromise between catalytic response/reproducibility, 9 μg of NM was selected for nano-StPEs FDH-biosensors development.

3.2. StPEs characterization

To investigate the morphology and electron-transfer features of the nanostructured StPEs, scanning electronic microscopy (SEM) and electrochemical impedance spectroscopy (EIS) were employed. Fig. 2A and **B** reports the SEM micrographs obtained at the StPE-CB and StPE-MS, respectively.

The surface of the nano-StPEs is composed of a continuous and homogeneous 0D-material layer with no macro holes and fractures. Looking at the micrographs magnifications (Fig. 2A and **B** insets) it is possible to appreciate the presence of nanosized particles with spherical shapes; they represent the CB and MS fundamental units confirming the 0D-nature of the water-prepared NMs.

The charge-transfer resistance (R$_{CT}$) of the StPEs transducers was studied via EIS; the resulting Nyquist plots are displayed in Fig. 2C. The contribution of the NMs in bringing down the R$_{CT}$ is clear. The pristine

StPE shows a wide semicircle characterized by an R$_{CT}$ of 594.6 ± 94.6 Ω; an additional shoulder at lower frequencies is also present due to the binders and plasticizers commonly present in inks (Wang et al., 1998; Yuan et al., 2021). On the other hand, the nano-StPEs highlight an order of magnitude decrease in the R$_{CT}$ (StPE-CB: 25.3 ± 4.5 Ω; StPE-MS: 38.9 ± 1.8 Ω), characterized by the reduction of the size of the semicircle and the disappearance of additional shoulders.

The data obtained endorse the effectiveness of the aqueous-phase NMs sonochemical preparation/nanostructuration as a strategy able to ensure competitive electrochemical features. These findings are in accordance with our previous studies, where the sonochemical approach has been tested and optimized, for 2D and 1D-NMs (Elfadil et al., 2023; Fiori et al., 2023; Qurat Ul Ain et al., 2021), and in particular with the here used 0D CB nanoparticles (Silveri et al., 2022). The sonochemical effect for the 0D-NMs can be resumed as follow: the high-power sonication treatment allows to 'reduce' the bulk material, nanoparticles aggregates, to the native nanoparticle units; once dispersed, the stabilizing molecule (sodium cholate) adheres to the surface of the nanoparticle ensuring the NM dispersion in the water-phase (Silveri et al., 2022). Since the result is a 0D-NM colloidal dispersion, a purification step via centrifugation to remove the excess stabilizer can be carried out, avoiding any interference of the latter on the overall electrochemical performance of the material. The sonochemical treatment ensures the material nanostructuration and purification, allowing also easily control of the nanomaterial 'concentration' to use for the sensor development; therefore, the proposed NMs preparation approach is particularly prone
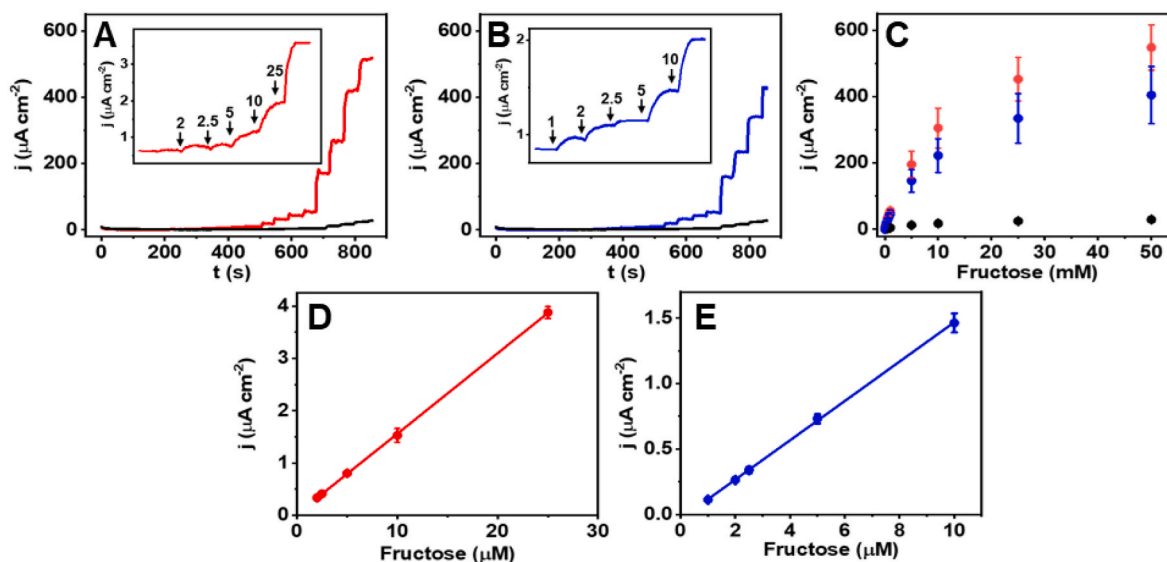

Fig. 3. Amperometric measurements obtained under continuous additions of D-fructose at increasing concentration at (**A**) StPE-CB (red curve) and (**B**) StPE-MS (blue curve), and bare-StPE (blue curves); measurements carried out at +0.15 V in ABS, D-fructose from 1 μM to 50 mM. (**C**) Dose-response plots obtained with the bare-StPE (black), StPE-CB (red curve) and StPE-MS (blue curve). Linear relationship between D-fructose concentration and current density for the (**D**) StPE-CB and (**E**) StPE-MS.
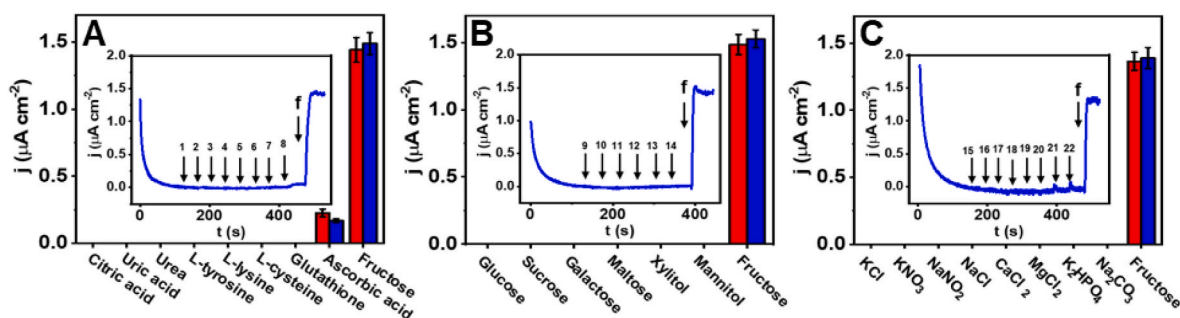
Fig. 4. Electrochemical response and relative amperometry plots (insets) obtained with the nano-StPEs (red bars: StPE-CB; blue bars: StPE-MS) under the continuous additions of potential interfering compounds belonging to different chemical classes. The 'f' indicates the addition of 10 μM D-fructose. (**A**) Organic compounds legend: 1 (100 μM citric acid), 2 (100 μM uric acid), 3 (1 mM urea), 4 (100 μM L-tyrosine), 5 (100 μM L-lysine), 6 (100 μM L-cysteine), 7 (100 μM glutathione), 8 (10 μM ascorbic acid). (**B**) Monosaccharides and disaccharides legend: 9 (1 mM D-glucose), 10 (1 mM sucrose), 11 (1 mM D-galactose), 12 (1 mM maltose), 13 (1 mM xylitol), 14 (1 mM Mannitol). (**C**) Electrolytes legend: 15 (1 mM KCl), 16 (1 mM KNO₃), 17 (1 mM NaNO₂), 18 (1 mM NaCl), 19 (1 mM CaCl₂), 20 (1 mM MgCl₂), 21 (1 mM K₂HPO₄), 22 (1 mM Na₂CO₃).

to electroanalytical purposes.

3.3. StPEs biosensing performance

FDH-based StPEs analytical features for D-fructose detection were extracted from amperometric measurements (performed under diffusion control) at $+0.15$ V (vs pseudo-Ag/AgCl) as working overpotential.

The influence of pH on the D-fructose catalytic response was investigated in the pH 3.0–6.0 range. Fig. S2 reveals that pH 4.5 is optimal to maximize enzymatic activity, exhibiting the highest and most reproducible catalytic current ($\Delta J_{cat} = 2.9 \pm 0.1$ μA cm^{-2}); while the signal progressively decreases till pH 6.0, according to the literature (Bollella et al., 2018a; Damar and Odaci Demirkol, 2011). The electroanalytical performance of the biosensors was investigated running amperometry under continuously increasing additions of D-fructose (from 1 μM to 50 mM). Fig. 3A and **B** report the amperometric curves obtained at the StPE-CB and StPE-MS, respectively; for comparison the signal obtained with the bare-StPE is also reported. Fig. 3C resumes the dose-response curves obtained with the three biosensors.

The previous trend observed with CVs was confirmed since both StPE-CB and StPE-MS returned a higher catalytic current compared to the bare lab-made sensor. Nevertheless, all StPEs exhibited similar Michaelis-Menten behaviors, with K_m^{app} values comparable with other FDH DET-based devices reported in the literature (Bolella et al., 2018b; Bollella et al., 2018a); the nano-StPEs J_{max} values result ~15 (StPEs-CB) and ~20 (StPEs-MS) folds higher than the pristine-StPE. The complete data set with the kinetic and electroanalytical parameters extrapolated are reported in Table S1. Two linear ranges were identified for each nanostructured biosensor, the latter are reported in Fig. 3D (2–25 μM) and **S3A** (50–500 μM) for StPE-CB, and Fig. 3E (1–10 μM) and **S3B** (25–250 μM) for StPE-MS. The limits of detection (LODs) and the sensitivity resulted to be 0.35 μM and 152.9 ± 2.8 μA cm^{-2} mM^{-1} for StPE-CB, and 0.16 μM and 149.6 ± 6.4 μA cm^{-2} mM^{-1} for StPE-MS. The LOD was calculated exploiting formula $3\sigma/m$, where σ is the standard deviation of the intercept, and m is the slope of the calibration curve.

The stability of the nano-StPEs response was assessed carrying out consecutive D-fructose chronoamperometric measurements. Fig. S4 demonstrates the satisfactory stability of both StPE-CB and StPE-MS, which returned repeatable signals up to ten consecutive measures (MS-SC: RSD = 3.9%; CB-SC RSD = 1.0%; n = 10). The reproducibility was assessed on calibration curves obtained with three independents biosensors; reproducible slopes for both linear ranges were obtained (StPE-CB: first linear range: 0.153 ± 0.003 μA cm^{-2} μM^{-1}, RSD = 1.9%; second linear range: 0.059 ± 0.002 μA cm^{-2} μM^{-1}, RSD = 4.9%. StPE-MS: first linear range: 0.150 ± 0.006 μA cm^{-2} μM^{-1}, RSD = 4.3%; second linear range: 0.070 ± 0.004 μA cm^{-2} μM^{-1}, RSD = 6.0%), demonstrating a satisfactory inter-electrode precision, and proving the

robustness of the whole biosensors fabrication strategy.

To better understand the obtained performance and the potentiality of the proposed nano-StPEs, Table S2 reported the comparison of the analytical figures of merit of FDH-based electrochemical biosensors reported in the literature (Antiochia and Gorton, 2014; Bolella et al., 2018b; Bollella et al., 2018a; Campuzano et al., 2003; Damar and Odaci Demirkol, 2011; Kinnear and Monbouquette, 1997; Nazaruk et al., 2014; Parellada et al., 1996; Šakinyte et al., 2015; Siepenkoetter et al., 2017; Suzuki et al., 2020). Looking at existing works, different nanostructured and porous materials have been employed to modify conventional electrochemical set-ups as glassy carbon, carbon paste, and gold electrodes; often it is reported the need for chemical modifiers to orient the redox protein and enhance performance. The proposed nano-StEPs allow to achieve better performance in terms of LOD, and sensitivity and linear range comparable to existing works; the better LOD can be attributed to the nano-StEPs ability to improve the electronic communication with FDH. The stencil-printed electrodes (after the modification with the nanomaterials) stability has been proved for two months (Silveri et al., 2022).

3.4. Selectivity study and samples analysis

The consumption of food and beverages with high sugar content significantly increased the risk of diabetes and cardiovascular diseases (Bray and Popkin, 2013); several studies have linked fructose to metabolic syndromes, through the promotion of insulin resistance in liver. Moreover, fructose can lead to the development of obesity, and several studies associate high levels of fructose intake during pregnancy and lactation with the development of metabolic dysfunctions (Sloboda et al., 2014). Hence rapid and in situ determination of fructose in food and biological fluids is of critical importance.

Thus, the nano-StEPs were challenged as independent measurement systems for the analysis of fructose in real samples. At first the selectivity was investigated, to evaluate the influence of potentially interfering species commonly present in food, beverages, and biological matrices. To this aim, the amperometric response of the nano-StPEs has been recorded in presence of organic compounds (Fig. 4A), mono/di-saccharides (Fig. 4B), and ions (Fig. 4C), evaluating also the D-fructose sensing ability in the solution.

Overall, the performances of both biosensors are not affected by the presence of potentially electro-active compounds due to the remarkable electrocatalytic features that allow working at low overpotential; no signal variation was detected due to inorganic ions. On the other hand, the selectivity in the presence of sugars depends mainly on the high specificity of the FDH active site, proving the specificity of the biorecognition event towards D-fructose. In particular, it is correct to discuss the slight signal obtained for ascorbic acid, which returns a
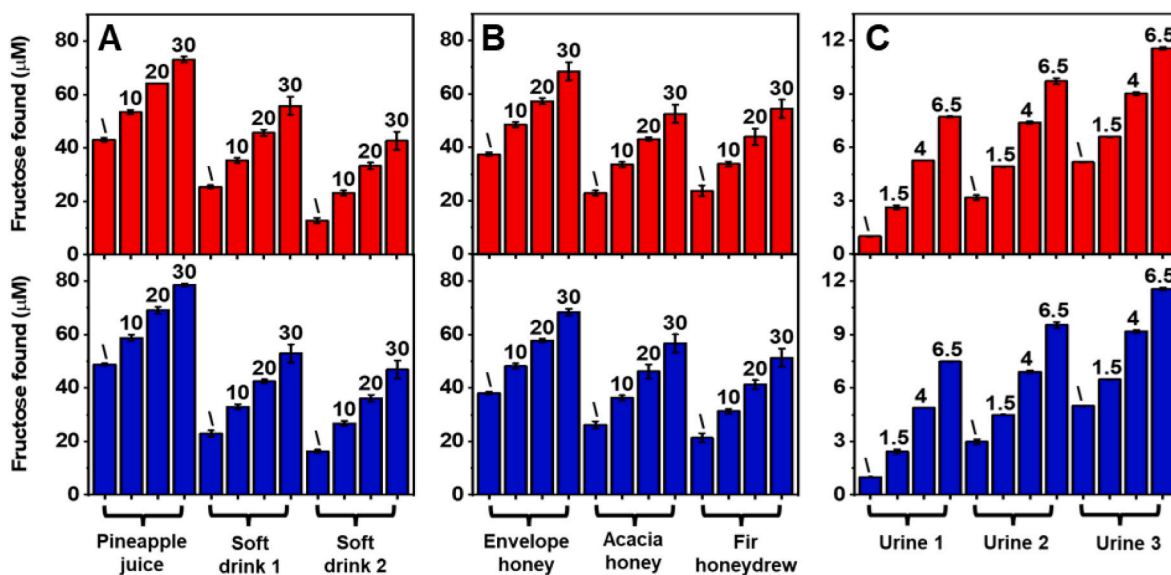
Fig. 5. Data obtained for real samples analysis performed with the StPE-CB (red bars) and StPE-MS (blue bars) analyzing (**A**) beverages, (**B**) honey, and (**C**) human urines; the labels on the bars represent the amount (in μM) of D-fructose added for recoveries studies. Dilution factor sample:ABS (v/v): pineapple juice and soft drinks 1:10,000; envelope honey 1:100,000; acacia honey and fir honey drew 1:200,000; urine 1:100.

response of ~15% compared to the D-fructose; nonetheless, considering the amount of ascorbic acid and D-fructose in the samples analyzed (Hounhouigan et al., 2014; Mênouwesso et al., 2020; Rumsey and Levine, 1998), and the dilution factor needed to analyze the samples (see below), the ascorbic acid in the samples can be considered at a non-interference level.

Three different commercial beverages and honey varieties were collected as samples; urine from healthy volunteers has been spiked at pathological and subpathological levels (100, 300, and 500 μM) to simulate different severity of diabetes pathologic conditions (Kawasaki et al., 2002, 2012). Recovery studies were employed to evaluate the accuracy of the biosensors, standard additions method was used for the quantification. Fig. 5 displays the results obtained for the sample analysis and recovery studies; the detailed data are listed in Table S3, whereas Fig. S5 shows three examples of chronoamperometric plots obtained for the analysis of different samples.

Bar graphs clearly show how both nano-StPE biosensors can determine D-fructose in the different samples; the accuracy and precision of the biosensors are evident from the recoveries (StPE-CB: 116.1%–94.9%; StPE-MS: 105.0%–95.9%) and reproducibility (StPE-CB: RSD $\leq$8.6%; StPE-MS: RSD $\leq$8.0%) obtained.

4. Conclusions

A benchtop approach to produce in-series fructose dehydrogenase-based third-generation integrated biosensors onto flexible substrates has been successfully proposed. Stencil printing was employed to define the sensors' shape and xurography for insulation; green-produced 0D-carbonaceous NMs were strategically employed to boost electro-catalysis. The final result is a fully integrated portable electrochemical set-up, capable to host the FDH-DET event. The nano-StPE biosensors demonstrated competitive analytical performance and selectivity and were successfully employed to determine D-fructose in beverages, honey and urines. Despite surely a scaling-up to mass production is required, the here proposed biosensors result in an affordable (cost per device less than 0.01€) and effective alternative, to the expensive, cumbersome, and slow colorimetric/fluorimetric kits for the determination of fructose.

Summing up, the marriage between the versatility of the sensor's fabrication approach and the electro-catalytic features conferred by the water-dispersed 0D-NMs provides a reliable and customizable alternative for the development of PoC/PoN devices useable out-of-lab, pioneering the concept of within everyone's reach devices.

CRediT Author Statement

Filippo Silveri: Conceptualization, Methodology, Formal analysis, Investigation, Data curation, Writing – original draft, Visualization.

Davide Paolini: Conceptualization, Methodology, Formal analysis, Investigation, Data curation, Visualization.

Flavio Della Pelle: Conceptualization, Methodology, Validation, Formal analysis, Data curation, Writing – original draft, Writing – review & editing, Visualization, Supervision, Project administration.

Paolo Bollella: Conceptualization, Validation, Formal analysis, Data curation, Writing – review & editing, Supervision.

Annalisa Scroccarello: Methodology, Formal analysis, Investigation, Writing – review & editing, Visualization.

Yohei Suzuki: Investigation, Resources. Eole Fukawa: Investigation, Resources.

Keisei Sowa: Investigation, Resources, Writing – review & editing.

Cinzia Di Franco: Investigation, Resources. Luisa Torsi: Validation, Writing – review & editing, Supervision, Funding acquisition.

Dario Compagnone:: Conceptualization, Validation, Writing – review & editing, Visualization, Supervision, Project administration, Funding acquisition.

Declaration of competing interest

The authors declare that they have no known competing financial interests or personal relationships that could have appeared to influence the work reported in this paper.

Data availability

Data will be made available on request.

Appendix A. Supplementary data

Supplementary data to this article can be found online at https://doi.org/10.1016/j.bios.2023.115450.

References

Adachi, T., Kitazumi, Y., Shirai, O., Kano, K., 2020. Direct electron transfer-type bioelectrocatalysis of redox enzymes at nanostructured electrodes. Catalysts. https://doi.org/10.3390/catal10020236.

Ameyama, M., Shinagawa, E., Matsushita, K., Adachi, O., 1981. D-fructose dehydrogenase of Gluconobacter industrius: purification, characterization, and application to enzymatic microdetermination of D-fructose. J. Bacteriol. 145, 814–823. https://doi.org/10.1128/jb.145.2.814-823.1981.

Antiochia, R., Gorton, L., 2014. A new osmium-polymer modified screen-printed graphene electrode for fructose detection. Sensor. Actuator. B Chem. 195, 287–293. https://doi.org/10.1016/j.snb.2014.01.050.

Arduini, F., Cinti, S., Caratelli, V., Amendola, L., Palleschi, G., Moscone, D., 2019. Origami multiple paper-based electrochemical biosensors for pesticide detection. Biosens. Bioelectron. 126, 346–354. https://doi.org/10.1016/j.bios.2018.10.014.

Bartlett, P.N., Al-Lolage, F.A., 2018. There is no evidence to support literature claims of direct electron transfer (DET) for native glucose oxidase (GOx) at carbon nanotubes or graphene. J. Electroanal. Chem. 819, 26–37. https://doi.org/10.1016/j.jelechem.2017.06.021.

Bolella, P., Gorton, L., Antiochia, R., 2018a. Direct Electron Transfer of Dehydrogenases for Development of 3rd Generation Biosensors and Sensors. Sensors 18. https://doi.org/10.3390/s18051319.

Bolella, P., Hibino, Y., Kano, K., Gorton, L., Antiochia, R., 2018b. Enhanced DET of FDH rationally Immobilized on a 2-Aminoanthracene Diazonium Cation. ACS Catal. 8, 10279–10289.

Bollella, P., 2022. Enzyme-based amperometric biosensors: 60 years later … Quo Vadis? Anal. Chim. Acta 1234, 340517. https://doi.org/10.1016/j.aca.2022.340517.

Bollella, P., Boeva, Z., Latonen, R.M., Kano, K., Gorton, L., Bobacka, J., 2021. Highly sensitive and stable fructose self-powered biosensor based on a self-charging biosupercapacitor. Biosens. Bioelectron. 176, 112909. https://doi.org/10.1016/j.bios.2020.112909.

Bollella, P., Hibino, Y., Conejo-valverde, P., Soto-cruz, J., Bergueiro, J., 2019. The influence of the shape of Au nanoparticles on the catalytic current of fructose dehydrogenase. Anal. Bioanal. Chem. 7645–7657.

Bollella, P., Hibino, Y., Kano, K., Gorton, L., Antiochia, R., 2018a. Highly Sensitive Membraneless Fructose Biosensor Based on Fructose Dehydrogenase Immobilized onto Aryl Thiol Modified Highly Porous Gold Electrode: Characterization and Application in Food Samples. Anal. Chem. 90, 12131–12136. https://doi.org/10.1021/acs.analchem.8b03093.

Bollella, P., Hibino, Y., Kano, K., Gorton, L., Antiochia, R., Turner, C., Bergquist, J., 2018b. The influence of pH and divalent / monovalent cations on the internal electron transfer (IET), enzymatic activity , and structure of fructose dehydrogenase. Anal. Bioanal. Chem. 3253–3264.

Bollella, P., Katz, E., 2020. Enzyme-based biosensors: Tackling electron transfer issues. Sensors 20, 1–32. https://doi.org/10.3390/s20123517.

Bray, G.A., Popkin, B.M., 2013. Calorie-sweetened beverages and fructose: what have we learned 10 years later. Pediatr. Obes. 242–248 https://doi.org/10.1111/j.2047-6310.2013.00171.x.

Bukhari, Q.U.A., Silveri, F., Della Pelle, F., Scroccarello, A., Zappi, D., Cozzoni, E., Compagnone, D., 2021. Water-Phase Exfoliated Biochar Nanofibers from Eucalyptus Scraps for Electrode Modification and Conductive Film Fabrication. ACS Sustain. Chem. Eng. 9, 13988–13998. https://doi.org/10.1021/acssuschemeng.1c05893.

Byakodi, M., Shrikrishna, N.S., Sharma, R., Bhansali, S., Mishra, Y., Kaushik, A., Gandhi, S., 2022. Emerging 0D, 1D, 2D, and 3D nanostructures for efficient point-of-care biosensing. Biosens. Bioelectron. X 12, 100284. https://doi.org/10.1016/j.biosx.2022.100284.

Campuzano, S., Gálvez, R., Pedrero, M., De Villena, F.J.M., Pingarrón, J.M., 2003. An integrated electrochemical fructose biosensor based on tetrathiafulvalene-modified self-assembled monolayers on gold electrode. Anal. Bioanal. Chem. 377, 600–607. https://doi.org/10.1007/s00216-003-2123-7.

Campuzano, S., Pedrero, M., Yáñez-Sedeño, P., Pingarrón, J.M., 2021. New challenges in point of care electrochemical detection of clinical biomarkers. Sensor. Actuator. B Chem. 345 https://doi.org/10.1016/j.snb.2021.130349.

Chekin, F., Gorton, L., Tapsobea, I., 2015. Direct and mediated electrochemistry of peroxidase and its electrocatalysis on a variety of screen-printed carbon electrodes : amperometric hydrogen peroxide and phenols biosensor. Anal. Bioanal. Chem. 439–446. https://doi.org/10.1007/s00216-014-8282-x.

Cinti, S., 2019. Novel paper-based electroanalytical tools for food surveillance. Anal. Bioanal. Chem. 411, 4303–4311 411 (2019) doi:10.1007/s00216-019-01640-5.

Damar, K., Odaci Demirkol, D., 2011. Modified gold surfaces by poly(amidoamine) dendrimers and fructose dehydrogenase for mediated fructose sensing. Talanta 87, 67–73. https://doi.org/10.1016/j.talanta.2011.09.042.

Elfadil, D., Silveri, F., Palmieri, S., Della, F., Sergi, M., Del, M., Amine, A., Compagnone, D., 2023. Liquid-phase exfoliated 2D graphene nanoflakes electrochemical sensor coupled to molecularly imprinted polymers for the determination of citrinin in food. Talanta 253, 124010. https://doi.org/10.1016/j.talanta.2022.124010.

Fiori, S., Della Pelle, F., Silveri, F., Scroccarello, A., Cozzoni, E., Del Carlo, M., Compagnone, D., 2023. Nanofibrillar biochar from industrial waste as hosting network for transition metal dichalcogenides. Novel sustainable 1D/2D nanocomposites for electrochemical sensing. Chemosphere 317, 137884. https://doi.org/10.1016/j.chemosphere.2023.137884.

Gooding, J.J., Ciampi, S., Gooding, J.J., 2011. The molecular level modification of surfaces : from self-assembled monolayers to complex molecular assemblies. Chem. Soc. Rev. 2704–2718. https://doi.org/10.1039/c0cs00139b.

Hernández-Rodríguez, J.F., Della Pelle, F., Rojas, D., Compagnone, D., Escarpa, A., 2020. Xurography-Enabled Thermally Transferred Carbon Nanomaterial-Based Electrochemical Sensors on Polyethylene Terephthalate-Ethylene Vinyl Acetate Films.Anal. Chem 92, 13565–13572. https://doi.org/10.1021/acs.analchem.0c03240.

Hiraka, K., Tsugawa, W., Asano, R., Yokus, M.A., Ikebukuro, K., Daniele, M.A., Sode, K., 2021. Rational design of direct electron transfer type L-lactate dehydrogenase for the development of multiplexed biosensor. Biosens. Bioelectron. 176, 112933. https://doi.org/10.1016/j.bios.2020.112933.

Hounhouigan, M.H., Linnemann, A.R., Soumanou, M.M., Van Boekel, M.A.J.S., 2014. Effect of Processing on the Quality of Pineapple Juice. Food Rev. Int. 30, 112–133. https://doi.org/10.1080/87559129.2014.883632.

Jayakumar, K., Reichhart, T.M.B., Schulz, C., Schulz, C., Felice, A.K.G., Leech, D., 2022. An Oxygen Insensitive Amperometric Glucose Biosensor Based on An Engineered Cellobiose Dehydrogenase: Direct versus Mediated Electron Transfer Responses. Chemelectrochem 9, e202200418. https://doi.org/10.1002/celc.202200418.

Jeerapan, I., Sempionatto, J.R., Wang, J., 2020. On-Body Bioelectronics: Wearable Biofuel Cells for Bioenergy Harvesting and Self-Powered Biosensing. Adv. Funct. Mater. 30 https://doi.org/10.1002/adfm.201906243.

Kawai, S., Goda-Tsutsumi, M., Yakushi, T., Kano, K., Matsushita, K., 2013. Heterologous overexpression and characterization of a flavoprotein-cytochrome c complex fructose dehydrogenase of Gluconobacter japonicus NBRC3260. Appl. Environ. Microbiol. 79, 1654–1660. https://doi.org/10.1128/AEM.03152-12.

Kawasaki, T., Akanuma, H., Yamanouchi, T., 2002. Increased fructose concentrations in blood and urine in patients with diabetes. Diabetes Care 25, 353–357. https://doi.org/10.2337/diacare.25.2.353.

Kawasaki, T., Igarashi, K., Ogata, N., Oka, Y., Ichiyanagi, K., Yamanouchi, T., 2012. Markedly increased serum and urinary fructose concentrations in diabetic patients with ketoacidosis or ketosis.Acta. Diabetol 49, 119–123. https://doi.org/10.1007/s00592-010-0179-3.

Kay, R., Desmulliez, M., 2012. A review of stencil printing for microelectronic packaging. Solder. Surf. Mt. Technol. 24, 38–50. https://doi.org/10.1108/09540911211198540.

Khodabakhshi, S., Fulvio, P.F., Andreoli, E., 2020. Carbon black reborn: Structure and chemistry for renewable energy harnessing. Carbon N. Y. 162, 604–649. https://doi.org/10.1016/j.carbon.2020.02.058.

Kinnear, K.T., Monbouquette, H.G., 1997. An Amperometric Fructose Biosensor Based on Fructose Dehydrogenase Immobilized in a Membrane Mimetic Layer on Gold. Anal. Chem. 69, 1771–1775. https://doi.org/10.1021/ac960665c.

Kong, X., Gai, P., Ge, L., Li, F., 2020. Laser-Scribed N-Doped Graphene for Integrated Flexible Enzymatic Biofuel Cells. ACS Sustain. Chem. Eng. 8, 12437–12442. https://doi.org/10.1021/acssuschemeng.0c03051.

Kongkaew, S., Tubtimtong, S., Thavarungkul, P., Kanatharana, P., Chang, K.H., Abdullah, A.F.L., Limbut, W., 2022. A Fabrication of Multichannel Graphite Electrode Using Low-Cost Stencil-Printing Technique. Sensors 22, 1–13. https://doi.org/10.3390/s22083034.

Li, X., Zhang, M., Hu, Y., Xu, J., Sun, D., Hu, T., Ni, Z., 2020. Developing a versatile electrochemical platform with optimized electrode configuration through screen-printing technology toward glucose detection. Biomed. Microdevices 22. https://doi.org/10.1007/s10544-020-00527-y.

Loew, N., Shitanda, I., Goto, H., Watanabe, H., Mikawa, T., Tsujimura, S., Itagaki, M., 2022. High-performance paper-based biocathode fabricated by screen-printing an improved mesoporous carbon ink and by oriented immobilization of bilirubin oxidase. Sci. Rep. 12, 1–14. https://doi.org/10.1038/s41598-022-19052-4.

Mathew, M., Radhakrishnan, S., Vaidyanathan, A., Chakraborty, B., Rout, C.S., 2020. Flexible and wearable electrochemical biosensors based on two-dimensional materials: Recent developments. Anal. Bioanal. Chem. 1–36. https://doi.org/10.1007/s00216-020-03002-y.

Mènouwesso, H.H., Anita, R.L., Mohamed, M.S., Martinus, A.J.S.V.B., 2020. Effect of heat treatment on yeast inactivation, vitamin C and physicochemical quality of fresh pineapple juice. Afr. J. Food Sci. 14, 256–264. https://doi.org/10.5897/ajfs2020.1997.

Naghdi, T., Faham, S., Mahmoudi, T., Pourreza, N., Ghavami, R., Golmohammadi, H., 2020. Phytochemicals toward Green (Bio)sensing. ACS Sens 5, 3770–3805. https://doi.org/10.1021/acssensors.0c02101.

Nazaruk, E., Landau, E.M., Bilewicz, R., 2014. Membrane bound enzyme hosted in liquid crystalline cubic phase for sensing and fuel cells. Electrochim. Acta 140, 108–115. https://doi.org/10.1016/j.electacta.2014.05.130.

Nesakumar, N., Kesavan, S., Li, C.Z., Alwarappan, S., 2019. Microfluidic Electrochemical Devices for Biosensing. J. Anal. Test. 3, 3–18. https://doi.org/10.1007/s41664-019-0083-y.

Olloqui-Sariego, J.L., Calvente, J.J., Andreu, R., 2021. Immobilizing redox enzymes at mesoporous and nanostructured electrodes. Curr. Opin. Electrochem. 26, 100658. https://doi.org/10.1016/j.coelec.2020.100658.

Parellada, J., Domínguez, E., Fernández, V.M., 1996. Amperometric flow injection determination of fructose in honey with a carbon paste sensor based on fructose dehydrogenase.. Anal. Chim. Acta 330, 71–77. https://doi.org/10.1016/0003-2670(96)87686-0.

Park, J.A., Jung, S.M., Choi, J.W., Kim, J.H., Hong, S., Lee, S.H., 2018. Mesoporous carbon for efficient removal of microcystin-LR in drinking water sources, Nak-Dong River, South Korea: Application to a field-scale drinking water treatment. plant. Chemosphere 193, 883–891. https://doi.org/10.1016/j.chemosphere.2017.11.092.

Park, J.A., Jung, S.M., Yi, I.G., Choi, J.W., Kim, S.B., Lee, S.H., 2017. Adsorption of microcystin-LR on mesoporous carbons and its potential use in drinking water source. Chemosphere 177, 15–23. https://doi.org/10.1016/j.chemosphere.2017.02.150.

Qurat Ul Ain, B., Silveri, F., Della Pelle, F., Scroccarello, A., Zappi, D., Cozzoni, E., Compagnone, D., 2021. Water-Phase Exfoliated Biochar Nano fi bers from Eucalyptus Scraps for Electrode Modi fi cation and Conductive Film Fabrication. ACS Sustain. Chem. Eng. 9, 13988–13998. https://doi.org/10.1021/acssuschemeng.1c05893.

Rama, E.C., Abedul, M.T.F., 2021. Paper-Based Screen-Printed Electrodes: A New Generation of. Biosensors 11, 1–23.

Rojas, D., Della Pelle, F., Silveri, F., Ferraro, G., Fratini, E., Compagnone, D., 2022. Phenolic compounds as redox-active exfoliation agents for group VI transition metal dichalcogenides. Today Chem 26, 101122. https://doi.org/10.1016/j.mtchem.2022.10112.

Rojas, D., Hernández-Rodríguez, J.F., Della Pelle, F., Del Carlo, M., Compagnone, D., Escarpa, A., 2020. Oxidative stress on-chip: Prussian blue-based electrode array for in situ detection of H2O2 from cell populations. Biosens. Bioelectron. 170, 112669. https://doi.org/10.1016/j.bios.2020.112669.

Rumsey, S.C., Levine, M., 1998. Absorption, transport, and disposition of ascorbic acid in humans. J. Nutr. Biochem. 9, 116–130. https://doi.org/10.1016/S0955-2863(98)00002-3.

Šakinyte, I., Barkauskas, J., Gaidukevič, J., Razumiene, J., 2015. Thermally reduced graphene oxide: The study and use for reagentless amperometric d-fructose biosensors. Talanta 144, 1096–1103. https://doi.org/10.1016/j.talanta.2015.07.072.

Schachinger, F., Chang, H., Scheiblbrandner, S., Ludwig, R., 2021. Amperometric biosensors based on direct electron transfer enzymes. Molecules 26. https://doi.org/10.3390/molecules26154525.

Siepenkoetter, T., Salaj-Kosla, U., Magner, E., 2017. The Immobilization of Fructose Dehydrogenase on Nanoporous Gold Electrodes for the Detection of Fructose. ChemElectroChem 4, 905–912. https://doi.org/10.1002/celc.201600842.

Silva-Neto, H.A., Arantes, I.V.S., Ferreira, A.L., do Nascimento, G.H.M., Meloni, G.N., de Araujo, W.R., Paixão, T.R.L.C., Coltro, W.K.T., 2023. Recent advances on paper-based microfluidic devices for bioanalysis. TrAC, Trends Anal. Chem. 158 https://doi.org/10.1016/j.trac.2022.116893.

Silveri, F., Pelle, F. Della, Scroccarello, A., Mazzotta, E., Giulio, T. Di, Malitesta, C., Compagnone, D., 2022. Carbon Black Functionalized with Naturally Occurring Compounds in Water Phase for Electrochemical Sensing of Antioxidant Compounds. Antioxidants 11, 2008.

Sloboda, D.M., Li, M., Patel, R., Clayton, Z.E., Yap, C., Vickers, M.H., 2014. Early life exposure to fructose and offspring phenotype: Implications for long term metabolic homeostasis J. Obes. 2014 doi:10.1155/2014/203474.

Sugimoto, Y., Takeuchi, R., Kitazumi, Y., Shirai, O., Kano, K., 2016. Significance of mesoporous electrodes for noncatalytic faradaic process of randomly oriented redox proteins. J. Phys. Chem. C 120, 26270–26277. https://doi.org/10.1021/acs.jpcc.6b07413.

Suzuki, Y., Kano, K., Shirai, O., Kitazumi, Y., 2020. Diffusion-limited electrochemical D-fructose sensor based on direct electron transfer-type bioelectrocatalysis by a variant of D-fructose dehydrogenase at a porous gold microelectrode. J. Electroanal. Chem. 877, 114651. https://doi.org/10.1016/j.jelechem.2020.114651.

Suzuki, Y., Makino, Fumiaki, Miyata, Tomoko, Tanaka, Hideaki, Namba, Keiichi, Kano, Kenji, Sowa, Keisei, Kitazumi, Yuki, Shirai Suzuki, O.Y., Sowa, K., Kitazumi, Y., Shirai, O., Makino, F., Miyata, T., Namba, K., Tanaka, H., Kano, K., 2022. Structural and Bioelectrochemical Elucidation of Direct Electron Transfer-type Membrane-bound Fructose Dehydrogenase. ChemRxiv 1–5. doi:10.26434/chemrxiv-2022-d7hl9.

Tricase, A., Imbriano, A., Valentino, M., Ditaranto, N., Macchia, E., Franco, C. Di, Kidayaveettil, R., Leech, D., Piscitelli, M., Scamarcio, G., Perchiazzi, G., Torsi, L., Bollella, P., 2023. Water-Based Conductive Ink Formulations for Enzyme-Based Wearable Biosensors. Adv. Sens. Res. 2300036 1–10 doi:10.1002/adsr.202300036.

Umapathi, R., Ghoreishian, S.M., Rani, G.M., Cho, Y., Huh, Y.S., 2022. Review—Emerging Trends in the Development of Electrochemical Devices for the On-Site Detection of Food Contaminants. ECS Sensors Plus 1, 044601. https://doi.org/10.1149/2754-2726/ac9d4a.

Wang, J., Tian, B., Nascimento, V.B., Angnes, L., 1998. Performance of screen-printed carbon electrodes fabricated from different carbon inks. Electrochim. Acta 43, 3459–3465. https://doi.org/10.1016/S0013-4686(98)00092-9.

Wilson, G.S., 2016. Native glucose oxidase does not undergo direct electron transfer. Biosens. Bioelectron. 82, 7–8. https://doi.org/10.1016/j.bios.2016.04.083.

Xia, H. qi, Tang, H., Zhou, B., Li, Y., Zhang, X., Shi, Z., Deng, L., Song, R., Li, L., Zhang, Z., Zhou, J., 2020. Mediator-free electron-transfer on patternable hierarchical meso/macro porous bienzyme interface for highly-sensitive sweat glucose and surface electromyography monitoring. Sensor. Actuator. B Chem. 312 https://doi.org/10.1016/j.snb.2020.127962.

Yoon, H., Nah, J., Kim, H., Ko, S., Sharifuzzaman, M., Barman, S.C., Xuan, X., Kim, J., Park, J.Y., 2020. A chemically modified laser-induced porous graphene based flexible and ultrasensitive electrochemical biosensor for sweat glucose detection. Sensor. Actuator. B Chem 311, 127866. https://doi.org/10.1016/j.snb.2020.127866.

Yuan, X., Ma, L., Zhang, J., Zheng, Y., 2021. Simple pre-treatment by low-level oxygen plasma activates screen-printed carbon electrode: Potential for mass production. Appl. Surf. Sci. 544, 148760. https://doi.org/10.1016/j.apsusc.2020.148760.

Zavanelli, N., Kim, J., Yeo, W.H., 2021. Recent advances in high-throughput nanomaterial manufacturing for hybrid flexible bioelectronics. Materials (Basel) 14. https://doi.org/10.3390/ma14112973.

Zhang, S., Xie, Y., Feng, J., Chu, Z., Jin, W., 2021. Screen-printing of nanocube-based flexible microchips for the precise biosensing of ethanol during fermentation. AIChE J 67, 1–12. https://doi.org/10.1002/aic.17142.